Design and Analysis of a Rotor for a 22 kW Transversally Laminated Anisotropic Synchronous Reluctance Motor

Ali Ozdil[1, *], Yunus Uzun[2]
[1]*Department of Electrical-Electronics Engineering, Kirsehir Ahi Evran University, Kirsehir, Turkey*
[2]*Department of Electrical-Electronics Engineering, Aksaray University, Aksaray, Turkey*
ali.ozdil@ahievran.edu.tr

***Abstract*—Substantial increase in energy consumption in all around the world has led to researchers to need to produce electrical machines with high energy efficiency since majority of energy has been consumed at industry, especially by electrical machines. Among electrical machines, the Synchronous Reluctance Machines (SynRMs) have been preferred to investigate in recent years due to lack of Induction Machines (IMs) in terms of efficiency and high price of the Permanent Magnet Synchronous Machines (PMSMs). In this study, the Finite Element Analysis (FEA) showing the effects of phase angle of current, number of flux barriers, starting diameter of flux barriers, and ribs on machine performance of 22 kW Transversally Laminated Anisotropic (TLA)-SynRM with distributed winding have been carried out in ANSYS Electronics. The design is based on creating a novel rotor considering these rotor parameters since the utilized SynRM consists of same stator with same sized 22 kW IM. The performance of the machine has been investigated through torque, torque ripple, efficiency, saliency, and power factor. Moreover, the effect of the phase angle of the current on the machine performance and the comparison of the 22 kW-SynRM with the same sized and powered IM and with a different SynRM have been carried out in this study. This study has concluded that although the novel SynRM has high torque ripple values, it is better than the IM due to lack of copper losses of rotor and the previously utilized SynRM considering their efficiency classes. The efficiency class of novel SynRM is IE4, whereas that for utilized IM and previously created SynRM are IE1 and IE3, respectively.**

***Index Terms*—Average torque; Finite element method; Flux barrier numbers; Ribs; Phase angle of current; Synchronous reluctance motor.**

I. INTRODUCTION

Energy consumption is one of the major problems concerned of 21st century due to a considerable increment in energy demand. When energy consumption is regarded, electric motors are highly important as they are quite preferable in industry, expending almost 40 % of global energy [1]. To reduce this excessive consumption of electricity, creating energy efficient machines is crucial [2]. Among electrical machines, Induction Machines (IMs) are at the forefront with 87 % of market share [2] since they have a simple structure and their production costs are low [3]. However, they have some drawbacks: insufficient torque capability, low efficiency, high weight, and high losses [4], and therefore more efficient machines with higher torque capabilities are required. On the other hand, although Permanent Magnet Synchronous Machines (PMSMs) are highly efficient machines, utilization of high-cost magnets and productive dependency to a single country, China, have led researchers to produce alternative machines with lower price and comparable torque capability [5]. SynRMs are one of the most suitable candidates as an alternative to PMSMs since their production cost is low due to lack of magnets and they have comparable output torque with these machines.

The Synchronous Reluctance Machines have attractive features comparing with IMs and PMSMs: magnet free, hence lower production cost, having lack of rotor copper losses due to absence of winding in their rotor [6], high stability, high efficiency [7], and high torque/volume [8]. Moreover, SynRMs have cooler shaft and bearings leading to longer lifetime and low maintenance requirement because they do not include windings in their rotor [9]. Additionally, these machines can reach up to 82 % produced torque by IMs with 50 % less copper loss. Besides, SynRMs can generate 42 % higher torque with same copper losses [5] and this demonstrates how SynRMs are superior to IMs. Therefore, the analysis of these machines has been extensively accomplished in literature [3], [5], [9]–[11].

On the other hand, SynRMs suffer from high torque ripple and low power factor [12]. To overcome these disadvantages, the optimization of the rotor geometry is required [13], [14]. The aim of the optimization is to obtain appropriate rotor design with better power factor, lower torque ripple, and higher efficiency comparing with unoptimized structure.

In recent years, researchers have mainly focused on the design of rotor of SynRMs to obtain more efficient machines since they generally use the same stator with IMs

Manuscript received 26 February, 2021; accepted 30 May, 2021.
This work has been supported by the Research Fund of the Aksaray University (Project No. 2018/062).

[6], [15]. In some of these rotor designs, flux barriers and iron parts of rotor have been created using air and iron distribution concept spatially [16] and constructed according to the distribution of magnetomotive forces of *d*- and *q*-axis [17], [18]. Furthermore, to figure out effects of barrier shape to torque ripple and output torque of SynRMs, the machines with U-shaped and circular shaped rotors have been analysed in [15] and [14], respectively. Additionally, SynRMs with placed magnets in the certain parts of the flux barriers have been analysed in [19], [20]. Having considered rotor design, various optimization algorithms, such as Genetic Algorithm (GA) [21], Response Surface Method (RSM) [3], and Differential Evolution (DE) [22], have also been utilized to reduce torque ripple by researchers.

The cross section of the utilized TLA-type SynRM is illustrated in Fig. 1. The aim of this paper is to create an optimum rotor structure of TLA-type seen in Fig. 1, 22 kW SynRM that falls within IE4 Super-Premium efficiency class with an acceptable torque ripple considering the effects of phase angle of current, number of flux barriers, starting diameter of these barriers, and tangential and radial ribs on machine performance.

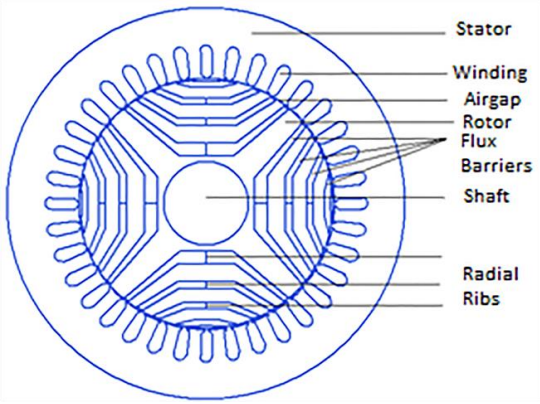

Fig. 1. The Cross section of TLA-type SynRM machines.

The specification of the novel SynRM is given in Table I. The difference of this study from the previous studies is that the efficiency class of the created SynRM, IE4 class, is 3-Class, and it is a class more efficient than the same sized and same powered IM and previously designed SynRM, respectively.

TABLE I. SPECIFICATION OF THE DESIGN.

Rated Power	22 kW
Rated Speed	1500 rpm
Rated Voltage	400 V
Winding Connection	Δ
Pole Number	4
Rated Frequency	50 Hz
Length of Stack	270 mm
Stator outer diameter	284 mm
Stator inner diameter	182.6 mm
Rotor outer diameter	181.6 mm
Rotor inner diameter	62 mm
Shaft diameter	31 mm
Airgap length	0.5 mm
Stacking Factor	0.95
Steel Type	M19_29G

The content of this study is as follows. Section I gives the theoretical background for the SynRMs; Section II explains the analytical design approach of these machines. The Finite Element Analysis is carried out in Section III, and finally, Section IV contains a Conclusion part of this study.

II. ANALYTICAL DESIGN APPROACH

A. Working Principle and Torque Generation of SynRM Machines

SynRMs are the members of the synchronous motor family based on the principle of the alternating current, which uses the same stator structure as IMs and generates an output torque based on the reluctance concept in their rotor. SynRMs utilize the concept of the interaction between the magnetic flux of the airgap and the rotating sinusoidal magnetomotive force (MMF) created from the windings in the stator [8]. The field produced by windings is transferred from stator to rotor through a small airgap. Moreover, the torque generation of these machines is based on the anisotropic geometry of rotor [5] and the equation for electromagnetic torque consists of the parameters: the saliency ratio, i.e., the ratio of *d*-axis inductance to *q*-axis inductance seen in (2) [23]. The determination of the saliency ratio, which is directly related to the torque generation of the motor, is provided with the help of flux barriers created in the rotor. Special positioning and sizing of air barriers directly affects the output torque, torque ripple, and other electrical and magnetic parameters of the machine. The number of poles and synchronous speed of the machine having three-phase standard asynchronous motor winding in its stator are determined depending on the number of rotor poles. Because SynRMs do not include permanent magnet, they cannot generate of magnet torque. Therefore, the electromagnetic torque, T_e, consists of only reluctance torque and it is defined by the difference of *d*-axis inductance, L_d, and *q*-axis inductance, L_q, given in (1) [24]

$$T_e = \frac{3}{2} p\ (L_d - L_q) I_d I_q, \tag{1}$$

where p is the number of pole pairs, I_d and I_q are the *d*- and *q*-axis currents, respectively. The electromagnetic torque can also be described as a function of saliency ratio given in (2), and it is shown in (3):

$$\zeta = \frac{L_d}{L_q}, \tag{2}$$

$$T_e = \frac{3}{2} p L_d \left(1 - \frac{1}{\zeta}\right) I_d I_q, \tag{3}$$

where ζ is the saliency ratio.

The output torque can also be obtained from the phase angle of current between *d*- and *q*- axis. Defining the produced airgap electromagnetic torque as a function of the phase angle of current, θ, shown in Fig. 2 is beneficial since controlling this angle is easier than that for current [25]. In the vector control of SynRMs, this angle provides optimum values of current vectors [26].

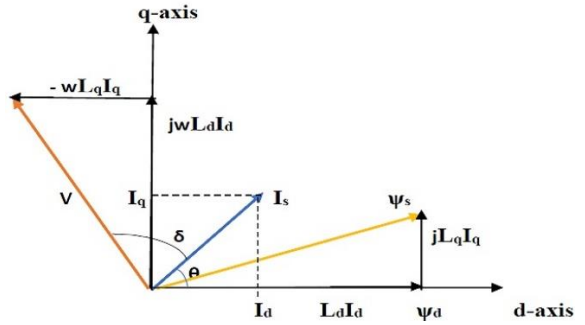

Fig. 2. Vector diagram of SynRMs.

The phase-angle-of-current-based torque expression is given in (4), and it is obtained by means of (5) and (6):

$$T_e = \frac{3}{2}\frac{p}{2}(L_d - L_q)\, I_s^2 \sin(2\theta), \tag{4}$$

$$I_d = I_s \cos(\theta), \tag{5}$$

$$I_q = I_s \sin(\theta). \tag{6}$$

Figure 2 and (4) demonstrate that the output torque is maximized when the phase angle of the current is 45 degrees for the certain stator current.

B. Types of SynRM

SynRMs are typically divided into three classes according to their rotor structure: Salient Pole, axially laminated anisotropic, ALA-type, and transversally laminated anisotropic, TLA-type, seen in Fig. 3.

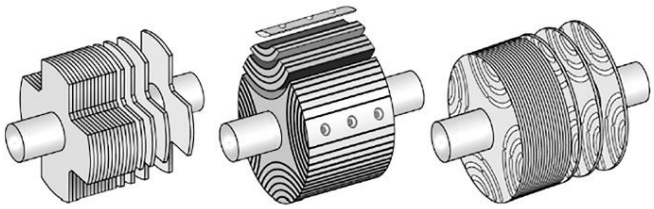
(a) (b) (c)

Fig. 3. Types of SynRM machines: a) Salient pole; b) ALA-type rotor; c) TLA-type rotor.

The first type of rotor structure is not commonly preferred due to its quite low saliency ratio and high harmonics [27]. On the other hand, high torque ripple and additional iron loss occur in the ALA-SynRMs [28], [29]. Although these types of machines are slightly more efficient than the TLA-type, TLA-SynRMs are superior to ALA-SynRMs in general since they have attractive features, such as stronger mechanical strength, better suitability to manufacture, easy to skew, cheaper production, and stronger mechanical strength [30], [31]. A TLA-SynRM has been analysed in this study due to these advantages.

C. Rotor Design of the TLA-SynRM

In this study, a 36-slots and 4-pole delta connected 22 kW SynRM with flux barriers has been analysed. Same stator structure and same winding scheme with 22 kW Inductance Machine have been utilized in this design of SynRM. Therefore, the evaluation of machine performance of this SynRM has been carried out based on the rotor design having main performance parameters as average output torque, torque ripple, efficiency, saliency, and power factor.

The basic rotor parameters that affect the performance of the machine are illustrated in Fig. 4. In this figure, R_b is the starting diameter of the flux barriers, B_0 is the flux barrier width, Y_0 is the segment width, W is the radial rib width, H is the tangential rib width, R is the rotor fillet radius, and R_0 is the barrier arch center location. Among these critical parameters, barrier and segment width are crucial since they define the insulation ratio of q-axes, $kwq = B_0/Y_0$, affecting the generated output torque significantly in SynRMs. Apart from these values, the airgap length, the shape of barriers, the barrier leg angle, and the phase angle of current are the parameters influencing the machine performance. However, they have not been analysed in detail in this study.

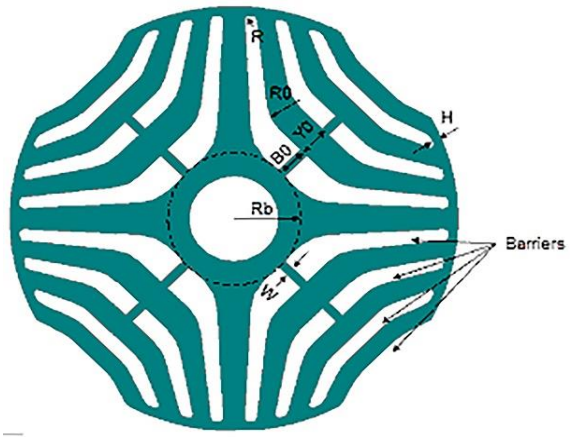

Fig. 4. The cross section of the core of the rotor of SynRM.

D. Performance Parameters

The average output torque, power factor, torque ripple, output power, losses, and efficiency are the performance parameters of SynRMs. Finding optimal values of all these parameters is quite challenging, and therefore some of these parameters are prioritized in SynRM designs. The aim of some designs is to obtain the maximum torque, whereas that of some others is to achieve maximum efficiency. Torque ripple and losses are parameters that affect machine performance negatively, therefore they must be kept at a minimum value.

The equations for T_e are given in (1) and (4). Because the output torque is created by means of the anisotropic rotor nature of SynRMs, these machines have a common drawback: torque ripple issues [26]. However, the anisotropic rotor structure causes to enhance the average value of T_e and the power factor [32] whose value is lower compared to IMs and PMSMs [33]. The power factor, PF, of the electrical machines can be obtained via (7)

$$PF = \cos(\varphi), \tag{7}$$

where Φ is the phase angle between the phase voltage and the phase current. The torque ripple of SynRMs can be basically obtained using (8) and given as

$$T_{rip}(\%) = \frac{T_{e(\max)} - T_{e(\min)}}{T_{avg}}. \tag{8}$$

Since the input power, P_{in}, is utilized while obtaining

efficiency values of SynRMs, the P_{in} of the three phase delta-connected SynRMs can be calculated from (9) as

$$P_{in} = 3V_s I_s \cos(\varphi), \tag{9}$$

where V_s and I_s are the phase voltage and the phase current, respectively. Moreover, the output power, P_{out}, of SynRMs is obtained from (10)

$$P_{out} = \omega_e T_e, \tag{10}$$

where w_e is the electrical speed of motor in rad/s. Losses are also crucial parameters in machine performance and they must be kept as low as possible during designs. The most dominant part of losses of SynRMs are copper losses, P_{copper}, and iron losses, P_{iron}, and they can be formulated in (11) and (12), respectively:

$$P_{copper} = 3R_s I_s^2, \tag{11}$$

$$P_{iron} = P_{hys} + P_{eddy} + P_{exc}, \tag{12}$$

where R_s is stator resistance, P_{hys}, P_{eddy}, and P_{exc} denote the hysteresis loss, eddy current loss, and excess loss, respectively. Hysteresis loss is dominant at low frequencies, whereas the other two losses are rulling at high frequencies [34].

Efficiency, η, of SynRM is found by the ratio of (11) to (10) and defined in (13)

$$\eta = \frac{P_{out}}{P_{in}} = \frac{P_{in} - P_{loss}}{P_{in}}, \tag{13}$$

where P_{loss} is the summation of P_{copper} and P_{iron}.

III. FINITE ELEMENT ANALYSIS

Insulation ratio and airgap length are crucial parameters in the design of SynRMs since the former significantly affects T_e and field produced in stator is transferred through the airgap. Having applied the parametric optimization to these parameters, the optimal airgap length and the insulation ratio of the motor have been found out as 0.5 mm and 0.7 mm respectively in this study. It should be stated that during the analysis of the effect of a parameter on machine performance, the other parameters have been kept constant to see the effect of the relevant parameter. The FEA analysis have been carried out in 2-D in ANSYS Electronics due to the requirement of less memory and less time. During the analysis, the Dirichlet boundary conditions have been used where vector potentials are assigned as 0 at the boundaries of rotor, stator, and shaft. These constant vector potentials ensure that the flux lines are parallel to the boundaries. Besides, the working temperature has been set as 75 °C. The dense mesh has been used in the air gap where electric field and potential changes are frequent, whereas the coarse mesh structure has been applied in regions where change occurs less, such as stator yoke. Moreover, analyses have been carried out in the 0 s–1 s interval and the number of parallel branches have been set as 2 in this study.

A. Phase Angle of Current Effect Analysis

This section includes the analysis of the phase angle of the current on machine performance parameters, efficiency and average output torque using 2D-FEA. Figure 5 shows the change of these two parameters according to that angle, θ, in between 25 and 60 degrees.

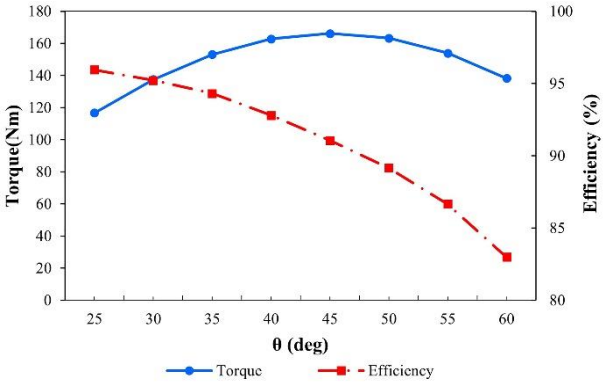

Fig. 5. Phase angle of current vs. efficiency and output torque.

Figure 5 illustrates that maximum torque is obtained at 45 degrees as mentioned in Section II-A and expressed in (4). However, the machine has the maximum efficiency as 95.95 % at 25 degrees of θ. As aforementioned in Section I, max T_e and the highest efficiency ratio, η, can be obtained at different θ.

The input and output powers of the machine also vary with the phase angle of current given in Table II. Table II demonstrates that the highest output power, P_{out}, is obtained when the phase angle of current is 45 degrees since machine operates in synchronism, and hence P_{out} directly depends on T_e seen in (10) and max value of T_e is obtained at that angle. Furthermore, P_{loss} can be obtained from Table II taking the difference between P_{out} and P_{in}. The table shows that total loss increases significantly with increments of θ.

TABLE II. EFFECT OF PHASE ANGLE OF CURRENT ON INPUT AND OUTPUT POWERS.

θ (°)	P_{in} (W)	P_{out} (W)
25	19103.6	18331.18
30	22696.8	21612.58
35	25498.7	24048.88
40	27558.9	25572.55
45	28669.2	26106.63
50	28467.9	25651.09
55	27893.9	24174.55
60	26179.0	21724.10

Though the machine has the highest efficiency ratio, i.e., 95.95 % at θ = 25 degrees, the angle of 30 degrees is the optimum value considering desired P_{out} of this study is 22 kW. Besides, the efficiency at 30 degrees is quite comparable with that for 25 degrees. For further analysis of this study, θ = 30 has been utilized.

The torque ripple values at a specified phase angle of current range varies in between 25 % and 45 %.

B. Effect of Number of Flux Barriers on Performance of the SynRM

Having obtained the optimum values of insulation ratio, airgap length, and phase angle of current from parametric

analysis, finding out the optimum number of flux barriers, B_s, is accomplished. In this part of the study, B_s = 1 and B_s = 2 have not been analysed due to their incompatible T_e and η values compared to 3, 4, and 5 barriers. Therefore, the effects of B_s varying in between 3 and 5 on T_e and η have been analysed and the results are demonstrated in Fig. 6. Moreover, P_{in} and P_{out} values at that barrier numbers are listed in Table III. The efficiency values of SynRM with 3, 4, and 5 barriers are calculated by means of the input and output powers given in this table.

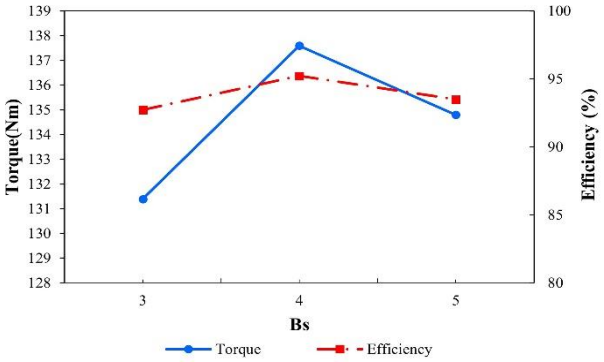

Fig. 6. Effect of barrier numbers on efficiency and torque.

TABLE III. EFFECT OF BARRIER NUMBERS ON INPUT AND OUTPUT POWERS.

B_s	P_{in} (W)	P_{out} (W)
3	22260.3	20638.68
4	22696.8	21612.58
5	22678.4	21173.23

Figure 6 demonstrates that increasing B_s from 3 to 4 leads to an increment in the machine efficiency 2.51 %, whereas enhancing B_s from 4 to 5 causes to 1.74 % reduction in machine efficiency. Figure 6 and Table III indicate that B_s = 4 has better characteristics than the others in terms of output torque and efficiency. Therefore, B_s = 4 is the optimum barrier number for the novel SynRM.

C. Effect of Starting Diameter of Flux Barriers on Performance of the SynRMs

The third step of this study is analysing the effect of the starting diameter of barriers on the SynRM's performance. Adjusting the starting diameter of SynRM is important since it helps to regulate the barrier end points which directly affect T_{rip} [35]. Since B_s = 4 is obtained as optimal barrier number for designed SynRM, the following analysis have been carried out based on that condition.

Figure 7 demonstrates that T_e decreases slightly as flux barriers move away from the shaft, whereas change in T_{rip} is nonlinear. Although the highest torque is obtained for R_b = 34 mm and the lowest T_{rip} occurs for R_b = 33 mm, the optimum starting diameter of barriers for this analysis is R_b = 35 mm since the machine reaches the highest efficiency at that value and there is insignificant difference between in T_e values. Apart from affecting T_e and η, R_b has influence on other machine performance parameters: P_{loss}, ζ, and, cos(Φ) demonstrated in Table IV.

Table IV shows that as starting diameter of flux barriers is further from the shaft, P_{loss} reduces since P_{copper} of stator (rotor has no copper loss in SynRMs) is dominant over P_{loss} and it highly depends upon I_s seen in (11) which also decreases with increment of R_b. Moreover, this table illustrates that changing R_b slightly effects ζ and cos(Φ).

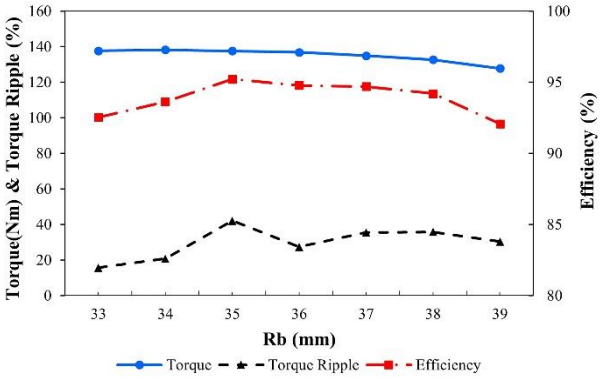

Fig. 7. Effect of starting diameters of barriers on efficiency, torque, and torque ripple.

TABLE IV. EFFECT OF STARTING DIAMETERS OF BARRIERS ON TOTAL LOSS, SALIENCY, AND POWER FACTOR.

R_b (mm)	P_{loss} (W)	Saliency	cos(Φ)
33	1456.5	12.40	0.784
34	1435.4	12.64	0.781
35	1405.4	12.76	0.768
36	1391.2	12.62	0.777
37	1373.4	12.49	0.772
38	1349.7	12.34	0.771
39	1315.7	12.15	0.773

D. Effects of Radial and Tangential Ribs on Performance of the SynRMs

The fourth FEA step of this study is analysing the individual effects of radial ribs in the q-axis, W, and tangential ribs, H, near the airgap on the SynRM's performance. These two parameters are prominent during the design of rotor of SynRMs because the seperation of segments in terms of magnetic point is carried out by these ribs. Moreover, ribs provide mechanical strength to the rotor and prevent barriers from breaking, however, they cause to increase in effects of saturation and cross-coupling in SynRMs.

Figure 8 illustrates the variation of T_e, η, and T_{rip} with W. According to this figure, efficiency values vary in the range of 94.5 % and 95.11 % in the parametric analysis. Efficiency increases 0.6 percent with 1.4 mm increment in radial rib width, whereas torque reduces about 13 % and torque ripple augments about 50 %. Though the highest torque is obtained for W = 0 mm, it cannot be considered as the most appropriate option among W values due to mechanical aspects and since η has the lowest value among the others.

From Table V, as radial ribs of flux barriers are wider, saliency decreases. Because the augmentation in rib width causes to a small decrease in L_d and an increase in L_q, and hence the reduction in saliency occurs. Moreover, cos(Φ) and P_{loss} declines with increment of W.

By considering Fig. 8 and Table V, W = 1 mm is achieved as the most appropriate radial rib width since the efficiency is the main concern of this study and it has the highest value at that rib width. Moreover, torque ripple is comparable with others, total power loss is low, and power factor at this rib

width slightly differs.

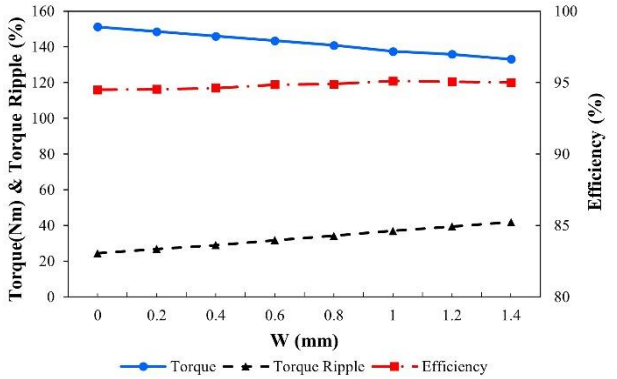

Fig. 8. Effect of radial ribs on efficiency, torque, and torque ripple.

TABLE V. EFFECT OF RADIAL RIBS ON TOTAL LOSS, SALIENCY, AND POWER FACTOR.

W (mm)	P_{loss} (W)	Saliency	cos(Φ)
0	1657.4	13.83	0.780
0.2	1607.1	13.61	0.779
0.4	1557.9	13.39	0.778
0.6	1511.2	13.14	0.775
0.8	1464.1	12.92	0.774
1	1408.4	12.69	0.772
1.2	1373.3	12.47	0.771
1.4	1331.3	12.23	0.770

Having accomplished the parametric analysis that W = 1 mm is found out as the optimal width for radial ribs, the effect of tangential ribs near the airgap has been analysed varying in between 0.6 mm and 2 mm in ANSYS Electronics. It should be considered that tangential ribs cannot be too narrow, generally should be more than 1 mm since cutting process of rotor is challenging for low tangential rib width, i.e., below 1 mm.

Figure 9 shows that as SynRM machines have wider tangential ribs, T_e decreases significantly due to L_d reduction caused by increasing cross-coupling of q-axis on d-axis, whereas their efficiency increases 3.4 % with 1.4 mm increment in the width of these ribs. However, it must be considered that increasing H induces a substantial decrement in P_{out} shown in Table VI. Besides, the output torque fluctuates nonlinearly with varied H values illustrated in Fig. 9.

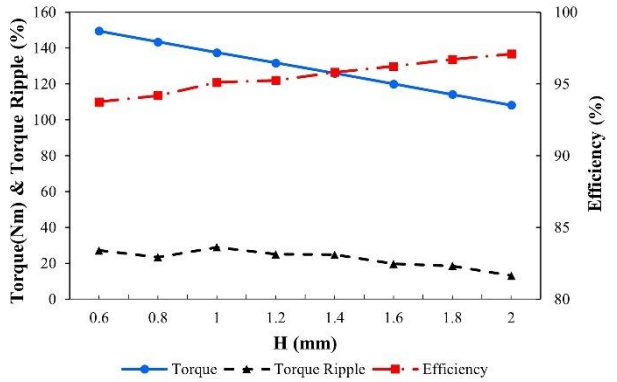

Fig. 9. Effect of tangential ribs on efficiency, torque, and torque ripple.

From Table VI, Saliency decreases almost 25 % as H increases from 0.6 mm to 2 mm because of aforementioned L_d reduction. In addition to that, reductions in P_{loss} and cos(Φ) occur when H is advanced (see Table VI).

TABLE VI. EFFECT OF TANGENTIAL RIBS ON OUTPUT POWER, TOTAL LOSS, SALIENCY, AND POWER FACTOR.

H (mm)	P_{out} (W)	P_{loss} (W)	Saliency	cos(Φ)
0.6	23477.64	1632.14	13.62	0.783
0.8	22539.99	1357.7	13.23	0.780
1	21601.58	1136.9	12.69	0.769
1.2	20698.53	1110.63	12.29	0.768
1.4	19786.04	876.08	11.79	0.764
1.6	18856.85	759.14	1129	0.759
1.8	17924.35	650.11	10.78	0.752
2	16998.84	543.82	10.26	0.746

Because the aim of this study is the analysis of 22 kW-SynRM machines, the optimal value for tangential ribs is H = 1 mm considering Fig. 9, Table VI, and mechanical aspects.

E. Comparison of 22 kW SynRM and IM

The final design of the novel SynRM is compared with an Induction Machine with same power, almost same output torque, same size, and same number of stator slots. In this FEM analysis, IM operates asynchronously at 1480 rpm considering slip effect, whereas SynRM works synchronously at 1500 rpm.

The examined parameters in FEM analysis to compare the performance of SynRM and IM are listed in Table VII.

TABLE VII. COMPARISON OF IM AND SYNRM MACHINES.

Performance Parameters	IM	SynRM
Speed	1480 rpm	1500 rpm
Frequency	50 Hz	50 Hz
Slip	1.33	0
Torque	137.55 Nm	137.52 Nm
Torque Ripple	17.43	28.03
Efficiency	89.35	95.11
Total Loss	1844.9 W	1136.9 W
Power Factor	0.809	0.768

IM has lower torque ripple than SynRM (Table VII). However, when the efficiency of the motors is considered, it is concluded that the efficiency of the Induction Motor is 89.35 %, which is in the range of IE1 efficiency class, while that for the novel SynRM is 95.11 %, which is in the range IE4 efficiency class. The design of a new rotor with substantially lower total loss due to no rotor copper loss in SynRM [36], [37].

IV. CONCLUSIONS

In this paper, the effects of the phase angle of current, flux barrier numbers, starting diameter of these barriers, radial and tangential ribs on performance of 22 kW-TLA type SynRM are analysed with FEA. Having obtained the most appropriate rotor geometry for this SynRM, the final design is compared with an IM having a same size, same power, and almost same output torque, and the results are demonstrated in Table VII. According to this table, although 22 kW Induction Machine is better than SynRM in terms of torque and torque ripple which is actually the main drawback of SynRMs, the novel SynRM satisfies 5.76 %

improvement in efficiency. This increased efficiency leads to that machine efficiency class is advanced from IE1 to IE4 class.

Besides, the total loss of SynRM is substantially less than that of IM due to having no copper loss. Apart from comparing with IM, the novel SynRM is more efficient than the SynRM created in [9] and [38]. Efficiency class stays remained in IE1 with 90.4 % in [9], and that for [38] switches for IE3 class with 92.5 %, whereas efficiency class of the novel SynRM is IE4 with 95.11 %, jumped 3-Class up.

CONFLICTS OF INTEREST

The authors declare that they have no conflicts of interest.

REFERENCES

[1] A. T. de Almeida, F. J. T. E. Ferreira, and G. Baoming, "Beyond induction motors - Technology Trends to move up efficiency", *IEEE Transactions on Industry Applications*, vol. 50, no. 3, pp. 2103–2114, May–Jun. 2014. DOI: 10.1109/TIA.2013.2288425.

[2] M. A. Kabir and I. Husain, "Design of synchronous reluctance motor with multilayer AC winding", in *Proc. of 2017 IEEE International Electric Machines and Drives Conference (IEMDC)*, 2017, pp. 1–7. DOI: 10.1109/IEMDC.2017.8002131.

[3] J.-K. Lee, D.-H. Jung, J. Lim, K.-D. Lee, and J. Lee, "A study on the synchronous reluctance motor design for high torque by using RSM", *IEEE Transactions on Magnetics*, vol. 54, no. 3, pp. 1–5, Mar. 2018, art. no. 8103005. DOI: 10.1109/TMAG.2017.2749325.

[4] A. Boglietti and M. Pastorelli, "Induction and synchronous reluctance motors comparison", in *Proc. of 2008 34th Annual Conference of IEEE Industrial Electronics*, 2008, pp. 2041–2044. DOI: 10.1109/IECON.2008.4758270.

[5] S. Panda, R. K. Keshri, and A. Vidyadharan, "Design and fabrication of synchronous reluctance motor for light electric vehicle applications", in *Proc. of 2019 IEEE Transportation Electrification Conference (ITEC-India)*, 2019, pp. 1–6. DOI: 10.1109/ITEC-India48457.2019.ITECINDIA2019-38.

[6] M. M. R. Sankestani and A. Siadatan, "Design of outer rotor synchronous reluctance motor for scooter application", in *Proc. of 2019 10th International Power Electronics, Drive Systems and Technologies Conference (PEDSTC)*, 2019, pp. 132–137. DOI: 10.1109/PEDSTC.2019.8697636.

[7] I.-H. Lin, M.-F. Hsieh, H.-F. Kuo, and M.-C. Tsai, "Improved accuracy for performance evaluation of synchronous reluctance motor", *IEEE Transactions on Magnetics*, vol. 51, no. 11, pp. 1–4, Nov. 2015, art. no. 8113404. DOI: 10.1109/TMAG.2015.2450255.

[8] L. Lavrinovicha and J. Dirba, "Comparison of permanent magnet synchronous motor and synchronous reluctance motor based on their torque per unit volume", in *Proc. of 2014 Electric Power Quality and Supply Reliability Conference (PQ)*, 2014, pp. 233–236. DOI: 10.1109/PQ.2014.6866817.

[9] A. V. Zakharov, S. I. Malafeev, and A. L. Dudulin, "Synchronous reluctance motor: Design and experimental research", in *Proc. of 2018 X International Conference on Electrical Power Drive Systems (ICEPDS)*, 2018, pp. 1–4. DOI: 10.1109/ICEPDS.2018.8571500.

[10] X. Diao, H. Zhu, Y. Qin, and Y. Hua, "Torque ripple minimization for bearingless synchronous reluctance motor", *IEEE Transactions on Applied Superconductivity*, vol. 28, no. 3, pp. 1–5, Apr. 2018, art no. 5205505. DOI: 10.1109/TASC.2018.2798632.

[11] V. Hrabovcova, P. Rafajdus, P. Lehocky, P. Makys, and M. Kremen, "Design of low voltage reluctance synchronous motor", in *Proc. of 2018 International Symposium on Electrical Machines (SME)*, 2018, pp. 1–6. DOI: 10.1109/ISEM.2018.8442705.

[12] S. Nattuthurai and R. Neelamegham, "Design and performance evaluation of SynRM and ferrite assisted-SynRM for EV application using FEA", in *Proc. of 2017 International Conference on Smart Technologies for Smart Nation (SmartTechCon)*, 2017, pp. 492–497. DOI: 10.1109/SmartTechCon.2017.8358422.

[13] Y. Okamoto, R. Hoshino, S. Wakao, and T. Tsuburaya, "Improvement of torque characteristics for a synchronous reluctance motor using MMA-based topology optimization method", *IEEE Transactions on Magnetics*, vol. 54, no. 3, pp. 1–4, Mar. 2018, art no. 7203104. DOI: 10.1109/TMAG.2017.2762000.

[14] R. Rouhani, S. E. Abdollahi, and S. A. Gholamian, "Torque ripple reduction of a synchronous reluctance motor for electric vehicle applications", in *Proc. of 2018 9th Annual Power Electronics, Drives Systems and Technologies Conference (PEDSTC)*, 2018, pp. 386–391. DOI: 10.1109/PEDSTC.2018.8343828.

[15] H. Yu, X. Zhang, J. Ji, and L. Xu, "Rotor design to improve torque capability in synchronous reluctance motor", in *Proc. of 2019 22nd International Conference on Electrical Machines and Systems (ICEMS)*, 2019, pp. 1–5. DOI: 10.1109/ICEMS.2019.8921518.

[16] Y. B. Yilmaz and E. Bostanci, "Effects of rotor flux barrier design on torque ripple and high speed performance of synchronous reluctance machines", in *Proc. of 2020 International Conference on Electrical Machines (ICEM)*, 2020, pp. 448–454. DOI: 10.1109/ICEM49940.2020.9270741.

[17] R.-R. Moghaddam, F. Magnussen, and C. Sadarangani, "Novel rotor design optimization of synchronous reluctance machine for low torque ripple", in *Proc. of 2012 XXth International Conference on Electrical Machines*, 2012, pp. 720–724. DOI: 10.1109/ICElMach.2012.6349952.

[18] R. R. Moghaddam, F. Magnussen, and C. Sadarangani, "Novel rotor design optimization of synchronous reluctance machine for high torque density", in *Proc. of 6th IET International Conference on Power Electronics, Machines and Drives (PEMD 2012)*, 2012, pp. 1–4. DOI: 10.1049/cp.2012.0256.

[19] P. Li, W. Ding, and G. Liu, "Sensitivity analysis and design of a high performance permanent-magnet-assisted synchronous reluctance motor for EV application", in *Proc. of 2018 IEEE Transportation Electrification Conference and Expo (ITEC)*, 2018, pp. 406–411. DOI: 10.1109/ITEC.2018.8450176.

[20] M. Ibrahim, F. Bernier, and J.-M. Lamarre, "Design of a PM-assisted synchronous reluctance motor utilizing additive manufacturing of magnetic materials", in *Proc. of 2019 IEEE Energy Conversion Congress and Exposition (ECCE)*, 2019, pp. 1663–1668. DOI: 10.1109/ECCE.2019.8912850.

[21] H.-s. Kim and B.-i. Kwon, "Optimal design of motor shape and magnetisation direction to obtain vibration reduction and average torque improvement in IPM BLDC motor", *IET Electric Power Applications*, vol. 11, no. 3, pp. 378–385, 2017. DOI: 10.1049/iet-epa.2016.0618.

[22] S. S. R. Bonthu and S. Choi, "Design procedure for multi-phase external rotor permanent magnet assisted synchronous reluctance machines", in *Proc. of 2016 IEEE Applied Power Electronics Conference and Exposition (APEC)*, 2016, pp. 1131–1137. DOI: 10.1109/APEC.2016.7468012.

[23] J. Lee *et al.*, "A study on analysis of synchronous reluctance motor considering axial flux leakage through end plate", *IEEE Transactions on Magnetics*, vol. 55, no. 6, pp. 1–4, Jun. 2019, art no. 8201704. DOI: 10.1109/TMAG.2019.2900737.

[24] S. E. Abdollahi, M. Mirzaei, and H. Lesani, "Rotor optimization of a segmented reluctance synchronous motor utilizing genetic algorithm", in *Proc. of 2009 International Conference on Electrical Machines and Systems*, 2009, pp. 1–4. DOI: 10.1109/ICEMS.2009.5382780.

[25] F.-J. Lin, M.-S. Huang, S.-G. Chen, C.-W. Hsu, and C.-H. Liang, "Adaptive backstepping control for synchronous reluctance motor based on intelligent current angle control", *IEEE Transactions on Power Electronics*, vol. 35, no. 7, pp. 7465–7479, Jul. 2020. DOI: 10.1109/TPEL.2019.2954558.

[26] C. Desai and P. Pillay, "Torque-angle characterization of a synchronous reluctance machine", in *Proc. of 2016 IEEE International Conference on Power Electronics, Drives and Energy Systems (PEDES)*, 2016, pp. 1–5. DOI: 10.1109/PEDES.2016.7914487.

[27] M. Hofer, M. Nikowitz, and M. Schrödl, "Comparative analysis of salient pole and flux barrier rotor for synchronous reluctance machines including flux weakening range", *The Journal of Engineering*, vol. 2019, pp. 4055–4059, 2019. DOI: 10.1049/joe.2018.8210.

[28] M. J. Kamper, F. S. Van der Merwe, and S. Williamson, "Direct finite element design optimisation of the cageless reluctance synchronous machine", *IEEE Transactions on Energy Conversion*, vol. 11, no. 3, pp. 547–555, Sept. 1996. DOI: 10.1109/60.537006.

[29] B. J. Chalmers and L. Musaba, "Design and field-weakening performance of a synchronous reluctance motor with axially-laminated rotor", in *IAS'97. Conference Record of the 1997 IEEE Industry Applications Conference Thirty-Second IAS Annual Meeting*, 1997, pp. 271–278, vol. 1. DOI: 10.1109/IAS.1997.643038.

[30] K. Chen, W. Yu, and C. Wen, "Rotor optimization for synchronous reluctance motors", *CES Transactions on Electrical Machines and*

Systems, vol. 3, no. 3, pp. 279–284, Sept. 2019. DOI: 10.30941/CESTEMS.2019.00036.

[31] A. Fratta, G. P. Troglia, A. Vagati, and F. Villata, "Evaluation of torque ripple in high performance synchronous reluctance machines", *Conference Record of the 1993 IEEE Industry Applications Conference Twenty-Eighth IAS Annual Meeting*, 1993, pp. 163–170, vol. 1. DOI: 10.1109/IAS.1993.298919.

[32] M. K. Lee and J. H. Lee, "Characteristics analysis of anisotropy rotor SynRM using a coupled FEM & Preisach model", in *Proc. of 2007 IEEE International Electric Machines & Drives Conference*, 2007, pp. 916–920. DOI: 10.1109/IEMDC.2007.382796.

[33] M. N. Ibrahim, P. Sergeant, and E. E. M. Rashad, "Combined star-delta windings to improve synchronous reluctance motor performance", *IEEE Transactions on Energy Conversion*, vol. 31, no. 4, pp. 1479–1487, Dec. 2016. DOI: 10.1109/TEC.2016.2576641.

[34] X. Ma, G. Li, Z. Zhu, G. Jewell, and J. Green, "Investigation on synchronous reluctance machines with different rotor topologies and winding configurations", *IET Electric Power Applications*, vol. 12, pp. 45–53, 2018. DOI: 10.1049/iet-epa.2017.0199.

[35] N. Bianchi, S. Bolognani, D. Bon, and M. D. PrÉ, "Torque harmonic compensation in a synchronous reluctance motor", *IEEE Transactions on Energy Conversion*, vol. 23, no. 2, pp. 466–473, Jun. 2008. DOI: 10.1109/TEC.2007.914357.

[36] P. Kostrauskas and A. Kalvaitis, "Electromagnetic torque of reluctance synchronous machine", *Elektron Elektrotech*, vol. 20, no. 2, Mar. 1999.

[37] A. Gencer, "Analysis and Control of Low-Voltage Ride-Through Capability Improvement for PMSG Based on an NPC Converter Using an Interval Type-2 Fuzzy Logic System", *Elektron Elektrotech*, vol. 25, no. 3, pp. 63-70, Jun. 2019. DOI: 10.5755/j01.eie.25.3.23678.

[38] M. Ersöz, Y. Öner, and O. Bingöl, "Akı bariyerli TLA tipi senkron relüktans motor tasarımı ve optimizasyonu", *Journal of the Faculty of Engineering and Architecture of Gazi University*, vol. 31, no. 4, pp. 941–950, 2016. DOI: 10.17341/gazimmfd.278449.